

Line-robust statistics for continuous gravitational waves: safety in the case of unequal detector sensitivities

David Keitel, Reinhard Prix

Albert-Einstein-Institut, Callinstrasse 38, 30167 Hannover, Germany

E-mail: david.keitel@aei.mpg.de, reinhard.prix@aei.mpg.de

published as Class. Quantum Grav. 32 035004, 5 January 2015

this version dated 15 January 2015

LIGO document number: LIGO-P1400161

Abstract. The multi-detector \mathcal{F} -statistic is close to optimal for detecting continuous gravitational waves (CWs) in Gaussian noise. However, it is susceptible to false alarms from instrumental artefacts, for example quasi-monochromatic disturbances ('lines'), which resemble a CW signal more than Gaussian noise. In a recent paper [1], a Bayesian model selection approach was used to derive line-robust detection statistics for CW signals, generalising both the \mathcal{F} -statistic and the \mathcal{F} -statistic consistency veto technique and yielding improved performance in line-affected data. Here we investigate a generalisation of the assumptions made in that paper: if a CW analysis uses data from two or more detectors with very different sensitivities, the line-robust statistics could be less effective. We investigate the boundaries within which they are still safe to use, in comparison with the \mathcal{F} -statistic. Tests using synthetic draws show that the optimally-tuned version of the original line-robust statistic remains safe in most cases of practical interest. We also explore a simple idea on further improving the detection power and safety of these statistics, which we however find to be of limited practical use.

Keywords: gravitational waves, signal processing, Bayesian inference, neutron stars

PACS numbers: 04.30.Tv, 04.80.Nn, 95.55.Ym, 97.60.Jd

1. Introduction

Continuous gravitational waves (CWs) are a potentially detectable class of astrophysical signals. They are narrow-band in frequency and can typically be described by a relatively stable signal model over years of observation [2, 3]. In the frequency band covered by terrestrial interferometric detectors (such as LIGO [4], Virgo [5] and GEO 600 [6]) CWs would be produced by rotating neutron stars with non-axisymmetric deformations [7–9].

Most CW data-analysis methods assume a Gaussian distribution for the detector noise. Indeed, in current interferometers this is a good description over most of the observation time and frequency range. (See, e.g., [10–12]). A standard detection statistic for CW signals in Gaussian noise is the \mathcal{F} -statistic, corresponding to a binary hypothesis test between a signal hypothesis and a Gaussian-noise hypothesis. Originally derived as a maximum-likelihood detection statistic [13, 14], it was also shown to follow from a Bayesian model-selection approach [15], using somewhat unphysical priors for the signal-amplitude parameters, which indicates that it is slightly suboptimal. Different choices of amplitude-parameter priors have been discussed in [15, 16], and a more physical reparametrisation was introduced in [17].

However, the detector data also contains non-Gaussian disturbances and *artefacts* of instrumental and environmental origin. CW searches are mainly affected by so-called ‘lines’: narrow-band disturbances that are present for a sizeable fraction of the observation time [11, 18–22].

Line artefacts are problematic because they can be ‘signal-like’ in the sense of being more similar to a CW signal than to Gaussian noise. Hence, they can cause significant outliers in a CW analysis that is based on the comparison of the signal model to Gaussian noise only leading to false alarms and therefore to decreased chances of detecting an actual signal.

Many ad-hoc approaches to mitigate the problem of lines have been developed in the past (see, e.g., [18, 19] and the references in section II.B of [1]). A Bayesian model-selection approach to line mitigation was first developed in [1]. The idea is to use a simple ‘signal-like’ model for line disturbances in a single detector. This does not require additional information about the characteristics of GW detectors, but only uses the main data stream already in use by the standard search methods, specifically the single- and multi-detector \mathcal{F} -statistics. Thus, it can be viewed as a generalisation of the \mathcal{F} -statistic consistency veto discussed and used in [11, 23, 24]. This way, *line-robust detection statistics* were derived, referred to in the following as O_{SL} and O_{SGL} in the notation of [1]. O_{SL} is specialised to the test of signals against lines, while O_{SGL} tests signals against a combined Gaussian noise + lines hypothesis, with a variable transition scale given by a parameter $\mathcal{F}_*^{(0)}$. This can be tuned empirically so that O_{SGL} reproduces the performance of the standard multi-detector \mathcal{F} -statistic in Gaussian data, but gives significant improvements in detection probability in line-affected frequency bands. We briefly summarise the definition of these statistics in section 2 of this paper.

In this paper, we investigate the behaviour of the line-robust statistics under a set of conditions which have not been tested in [1]. The idea of using a comparison between multi- and single-detector statistics, \mathcal{F} and \mathcal{F}^X , to distinguish CW signals from (non-coincident) lines implicitly relies on all detectors having similar sensitivities. Indeed, for the synthetic tests in [1] equal noise power spectral densities (PSDs) S^X were explicitly assumed, and in the tests on LIGO S5 data the largest deviation between the two detectors H1 and L1 was $\sqrt{S^{\text{H1}}}/\sqrt{S^{\text{L1}}} \approx 1.7$ (coherent example (b) in Table 1 of [1]). In addition, all tests so far have been for all-sky searches, averaging out the different antenna patterns of the individual detectors.

However, very different sensitivities could make signals and lines more difficult to distinguish by this method, because a signal may yield a significant outlier in only one detector and therefore appear ‘line-like’ for O_{SL} and O_{SGL} . This would lead to decreased detection power of the line-robust statistics both in the presence of lines and in pure Gaussian noise.

In section 3 we will investigate this concern about their *safety* under these generalised conditions, in the sense that they should never have worse detection probabilities than the standard \mathcal{F} -statistic. With numerical tests based on *synthetic draws* of \mathcal{F} -statistic values, it turns out that this issue only really affects O_{SL} and O_{SGL} with a transition-scale parameter $\mathcal{F}_*^{(0)}$ that is too low. An optimally-tuned O_{SGL} (in the sense of section VI.B of [1]) is found to be safe under most circumstances of practical relevance, though it can no longer provide improvements over \mathcal{F} in more extreme cases.

In section 4, we discuss an attempt to improve upon these statistics. Using a different amplitude-prior distribution than in [1], we obtain new per-detector sensitivity-weighting factors in the detection statistics, which depend on the noise PSDs, the amount of data and the sky-location-dependent detector responses. Synthetic tests show that this extra weighting does recover some of the losses of O_{SL} and of O_{SGL} tuned at relatively low $\mathcal{F}_*^{(0)}$, but that it brings no further improvement compared to an optimally-tuned O_{SGL} .

All numerical results in this paper are produced with the same synthesis approach as described in [1, 15, 16]. The discussion in this paper is limited to coherent statistics.

2. Summary of detection statistics

Here we give a short introduction to the various detection statistics considered here, which were discussed in more detail in [1]. These are based on comparing three different hypotheses about the observed data: a Gaussian noise hypothesis \mathcal{H}_{G} , a CW signal hypothesis \mathcal{H}_{S} and a simple non-coincident ‘line’ hypothesis \mathcal{H}_{L} .

This section also serves as an introduction to the notation used in this paper. By $x^X(t)$ we denote a time series of GW strain measured in a detector X . Following the multi-detector notation of [14, 25], boldface indicates a multi-detector vector, i.e., we write $\mathbf{x}(t)$ for the multi-detector data vector with components $x^X(t)$.

2.1. Posterior probabilities for the different hypotheses

Skipping the derivations given in [1], we start from the posterior probabilities. For the Gaussian-noise hypothesis, $\mathcal{H}_{\text{G}} : \mathbf{x}(t) = \mathbf{n}(t)$, we have

$$P(\mathcal{H}_{\text{G}}|\mathbf{x}) = \frac{P(\mathcal{H}_{\text{G}})}{P(\mathbf{x})} \kappa e^{-\frac{1}{2}(\mathbf{x}|\mathbf{x})}, \quad (1)$$

with a normalisation constant κ and a scalar product between time series defined as

$$(\mathbf{x}|\mathbf{y}) \equiv \sum_X \frac{1}{S^X} \int_0^T x^X(t) y^X(t) dt, \quad (2)$$

with the single-sided power-spectral densities S^X assumed as uncorrelated between different detectors X and constant over the (narrow) frequency band of interest.

For the signal hypothesis \mathcal{H}_{S} , a CW waveform $\mathbf{h}(t; \mathcal{A}, \lambda)$ is determined by four basis functions $\mathbf{h}_\mu(t; \lambda)$, the *amplitude parameters* \mathcal{A} and the *phase-evolution parameters* λ :

$$\mathcal{H}_{\text{S}} : \mathbf{x}(t) = \mathbf{n}(t) + \mathbf{h}(t; \mathcal{A}, \lambda) = \mathbf{n}(t) + \mathcal{A}^\mu \mathbf{h}_\mu(t; \lambda), \quad (3)$$

which is often referred to as the *JKS factorisation*, first introduced in [13].

For fixed λ and an amplitude-parameter prior distribution (as discussed in [1, 15, 16], and which we will revisit in section 4.1) of

$$P(\{\mathcal{A}^\mu\}|\mathcal{H}_S) = \begin{cases} C & \text{for } h_0^4(\mathcal{A}) < \frac{\hat{\rho}_{\max}^4}{\sqrt{|\mathcal{M}|}}, \\ 0 & \text{otherwise,} \end{cases} \quad (4)$$

with a free cut-off parameter $\hat{\rho}_{\max} \in (0, \infty)$, the posterior probability is

$$P(\mathcal{H}_S|\mathbf{x}) = o_{\text{SG}} \frac{70}{\hat{\rho}_{\max}^4} P(\mathcal{H}_G|\mathbf{x}) e^{\mathcal{F}(\mathbf{x})}, \quad (5)$$

with prior odds $o_{\text{SG}} \equiv P(\mathcal{H}_S)/P(\mathcal{H}_G)$, and the well-known multi-detector \mathcal{F} -statistic [13, 14] given by

$$2\mathcal{F}(\mathbf{x}) \equiv x_\mu \mathcal{M}^{\mu\nu} x_\nu, \quad (6)$$

with implicit summation over repeated amplitude indices μ, ν and the shorthand notations

$$x_\mu \equiv (\mathbf{x}|\mathbf{h}_\mu) \quad \text{and} \quad \mathcal{M}_{\mu\nu} \equiv (\mathbf{h}_\mu|\mathbf{h}_\nu). \quad (7)$$

For the line hypothesis \mathcal{H}_L , corresponding to $\mathcal{H}_L^X : x^X(t) = n^X(t) + h^X(t; \mathcal{A}^X)$ in an arbitrary single detector X , a similar derivation leads to

$$P(\mathcal{H}_L|\mathbf{x}) = \frac{70}{\hat{\rho}_{\max}^4} P(\mathcal{H}_G|\mathbf{x}) o_{\text{LG}} \left\langle r^X e^{\mathcal{F}^X(x^X)} \right\rangle_X, \quad (8)$$

where we define an average over detectors as

$$\langle Q^X \rangle_X \equiv \frac{1}{N_{\text{det}}} \sum_X Q^X, \quad (9)$$

and where again the prior-normalisation parameter $\hat{\rho}_{\max}$ appears. Through $o_{\text{LG}}^X \equiv P(\mathcal{H}_L^X)/P(\mathcal{H}_G^X)$ we have $o_{\text{LG}} \equiv \sum_X o_{\text{LG}}^X$ and, for N_{det} detectors:

$$r^X \equiv \frac{o_{\text{LG}}^X}{o_{\text{LG}}/N_{\text{det}}}, \quad \text{such that} \quad \sum_X r^X = N_{\text{det}}. \quad (10)$$

Furthermore, we can combine the (mutually exclusive) hypotheses \mathcal{H}_G and \mathcal{H}_L into an extended noise hypothesis $\mathcal{H}_{\text{GL}} \equiv (\mathcal{H}_G \text{ or } \mathcal{H}_L)$, with posterior probability

$$\begin{aligned} P(\mathcal{H}_{\text{GL}}|\mathbf{x}) &= P(\mathcal{H}_G|\mathbf{x}) + P(\mathcal{H}_L|\mathbf{x}) \\ &= P(\mathcal{H}_G|\mathbf{x}) \left(1 + \frac{70}{\hat{\rho}_{\max}^4} o_{\text{LG}} \left\langle r^X e^{\mathcal{F}^X(x^X)} \right\rangle_X \right). \end{aligned} \quad (11)$$

2.2. Odds ratios

These posterior probabilities can be used to compute odds ratios between the different hypotheses. First, we see from (1) and (5) that

$$O_{\text{SG}}(\mathbf{x}) \equiv \frac{P(\mathcal{H}_S|\mathbf{x})}{P(\mathcal{H}_G|\mathbf{x})} \propto e^{\mathcal{F}(\mathbf{x})}, \quad (12)$$

i.e., this Bayesian approach reproduces the \mathcal{F} -statistic as the optimal detection statistic for CW signals in pure Gaussian noise and under the prior (4).

Alternatively, using the posterior probabilities given by (5) and (8), we obtain the posterior signal-versus-line odds as

$$O_{\text{SL}}(\mathbf{x}) \equiv \frac{P(\mathcal{H}_{\text{S}}|\mathbf{x})}{P(\mathcal{H}_{\text{L}}|\mathbf{x})} = o_{\text{SL}} \frac{e^{\mathcal{F}(\mathbf{x})}}{\langle r^X e^{\mathcal{F}^X(x^X)} \rangle_X}, \quad (13)$$

with the prior odds $o_{\text{SL}} \equiv P(\mathcal{H}_{\text{S}})/P(\mathcal{H}_{\text{L}}) = o_{\text{SG}}/o_{\text{LG}}$. Note that the amplitude-prior cut-off $\hat{\rho}_{\text{max}}$ has disappeared, as we have used the same amplitude prior on lines and signals.

Finally, using (5) and (11), we obtain generalised signal-versus-noise odds

$$O_{\text{SGL}}(\mathbf{x}) = o_{\text{SGL}} \frac{e^{\mathcal{F}(\mathbf{x})}}{(1 - p_{\text{L}}) e^{\mathcal{F}_*^{(0)}} + p_{\text{L}} \langle r^X e^{\mathcal{F}^X(x^X)} \rangle_X}, \quad (14)$$

where we have rewritten some of the prior parameters in terms of the line probability

$$p_{\text{L}} \equiv P(\mathcal{H}_{\text{L}}|\mathcal{H}_{\text{GL}}) = \frac{o_{\text{LG}}}{1 + o_{\text{LG}}} \in [0, 1] \quad (15)$$

and a transition-scale parameter

$$\mathcal{F}_*^{(0)} \equiv \ln \frac{\hat{\rho}_{\text{max}}^4}{70}. \quad (16)$$

Note that, contrary to the previous odds O_{SG} and O_{SL} , now the choice of amplitude-prior cut-off parameter $\hat{\rho}_{\text{max}}$ will affect the properties of the resulting statistic. Methods for tuning these free parameters have been discussed in section VI.B of [1].

3. Safety of the line-robust statistics for unequal sensitivities

Consider a network of two detectors A and B, with A being much more sensitive than B. There may be CW signals that are strong enough to cause a significant outlier in the single-detector \mathcal{F}^{A} -statistic, but fail to do so in \mathcal{F}^{B} , because the signal is still buried in the higher noise level of detector B. For such a network, the multi-detector \mathcal{F} -statistic is dominated by the contribution from the more sensitive detector A, so that either for a signal or for a strong line in A, $\mathcal{F} \approx \mathcal{F}^{\text{A}}$ holds. Hence, in this case both an actual astrophysical CW signal and an instrumental line can have very similar signatures in terms of the set of values $\{\mathcal{F}, \mathcal{F}^X\} = \{\mathcal{F}, \mathcal{F}^{\text{A}}, \mathcal{F}^{\text{B}}\}$.

The line-veto statistic O_{SL} and line-robust statistic O_{SGL} , as given in (13) and (14), are intended to suppress 'signal-like' lines and thus they always include a test of tentative signals against the line hypothesis. If, however, weaker signals appear as 'line-like' in terms of $\{\mathcal{F}, \mathcal{F}^X\}$, those also receive low odds. Therefore, it can be expected that these statistics will have problems distinguishing lines from signals in such unequal-sensitivity cases, losing detection power due to increased false dismissals.

In order to quantify under which conditions a problem may occur, recall the definition of the multi-detector \mathcal{F} -statistic from (6). The sensitivity of a detector network is encoded in the antenna-pattern matrix $\mathcal{M}_{\mu\nu}$, which for high-frequency GWs is given approximately by [26]

$$\mathcal{M}_{\mu\nu} \approx \mathcal{S}^{-1} T_{\text{data}} \begin{pmatrix} A & C & 0 & 0 \\ C & B & 0 & 0 \\ 0 & 0 & A & C \\ 0 & 0 & C & B \end{pmatrix}, \quad (17)$$

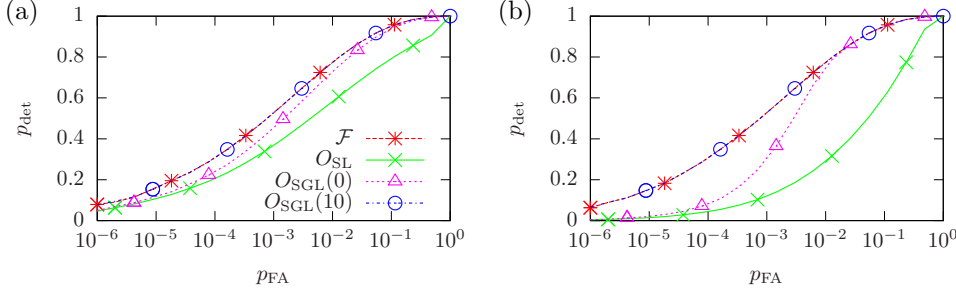


Figure 1. Receiver-operating characteristics (ROCs) for signals in pure Gaussian noise: Detection probability p_{det} as a function of false-alarm probability p_{FA} for different synthetic statistics, for detectors H1 and H2 and signals with $\rho_S = 4$ in Gaussian noise without line contamination. The panels show relative detector sensitivities of (a) $\sqrt{S^{\text{H2}}} = \sqrt{S^{\text{H1}}}$, (b) $\sqrt{S^{\text{H2}}} = 10\sqrt{S^{\text{H1}}}$. For O_{SGL} , different values of $\mathcal{F}_*^{(0)}$ are given in brackets.

and specifically in its determinant

$$|\mathcal{M}| \equiv \mathcal{S}^{-4} T_{\text{data}}^4 D^2. \quad (18)$$

Here, \mathcal{S} is the multi-detector noise PSD, T_{data} is the effective amount of data and $D \equiv AB - C^2$ quantifies the antenna-pattern-based sensitivity to a particular sky location. See Appendix A for full expressions of the *antenna-pattern matrix elements* A , B , C , D .

The corresponding single-detector quantity is

$$|\mathcal{M}^X| = \mathcal{S}^{-4} T_{\text{data}}^4 (D^X)^2, \quad (19)$$

where D^X , through the noise-weighted average from (A.10), depends quadratically on $(S^X)^{-1}$ and T_{data}^X . Example plots for $D^X(\alpha, \delta)$ are also given in Appendix A.

Thus, for two given detectors, their relative sensitivities are given by their noise PSDs S^X , their amounts of data T_{data}^X and the relative sky-position sensitivities D^X . In the following, we will only consider the first and third contribution, since T_{data}^X enters to the same power as $(S^X)^{-1}$ and is therefore equivalent to a corresponding change in that quantity. We first consider the case of two colocated detectors, for example LIGO H1 and H2 at Hanford (Washington state), for different S^X and various noise distributions, in sections 3.1–3.3, and then the case of non-colocated detectors (LIGO H1 and L1 at Livingston, Louisiana) with different D^X in section 3.4.

Here and in section 4.5, O_{SL} and O_{SGL} use (truncated) ‘perfect-knowledge’ line priors: $o_{\text{LG}}^X = \max\{0.001, f_L^X / (1 - f_L^X)\}$ for a *line-contamination fraction* f_L^X , i.e. when a percentage f_L^X of noise candidates in detector X comes from lines and the complement comes from pure Gaussian noise. All receiver-operating characteristic (ROC) curves – comparisons of detection probabilities p_{det} as a function of false-alarm probability p_{FA} – are based on $N_{\text{draws}} = 10^7$ each for noise and signal populations, while the two-dimensional parameter-space exploration plots have $N_{\text{draws}} = 10^5$ per parameter combination.

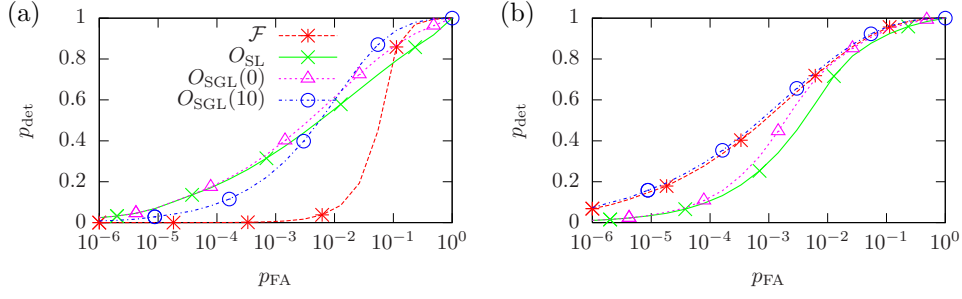


Figure 2. Lines in the less sensitive detector: ROCs for an H1-H2 network, signals with $\rho_S = 4$ and line-contamination fraction $f_L^{H2} = 0.1$, with $\rho_L = 6$. The panels show relative detector sensitivities of (a) $\sqrt{S^{H2}} = \sqrt{S^{H1}}$, (b) $\sqrt{S^{H2}} = 10\sqrt{S^{H1}}$.

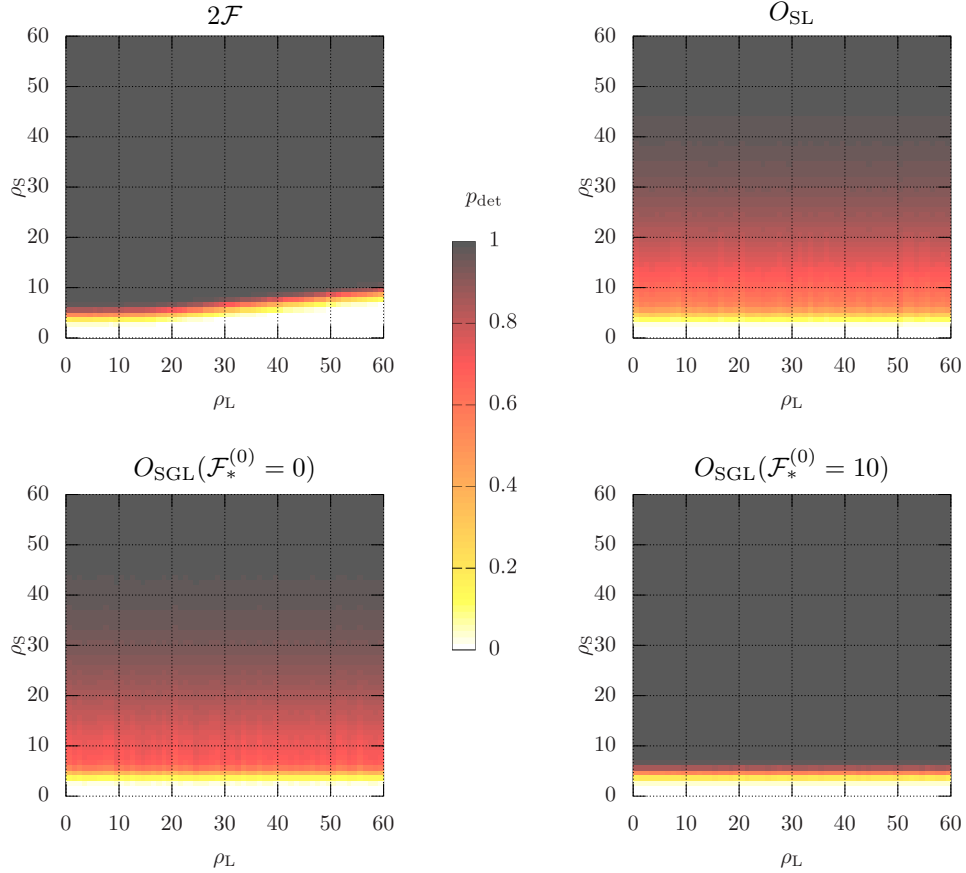


Figure 3. Lines in the less sensitive detector: detection probabilities p_{det} of different statistics, for an H1-H2 network with $\sqrt{S^{H2}} = 10\sqrt{S^{H1}}$, as a function of line SNR ρ_L and signal SNR ρ_S at fixed line contamination $f_L^{H2} = 0.1$ and false-alarm probability $p_{\text{FA}} = 0.001$.

3.1. Gaussian noise

ROC curves for synthetic draws from a signal population with fixed signal-to-noise ratio (SNR) of $\rho_S = 4$ and pure Gaussian noise without line contamination are shown in figure 1. In panel (a), both detectors have the same PSD, $\sqrt{S^{H2}} = \sqrt{S^{H1}}$. The results are very similar to those from [1], where an H1-L1 network was used with identical parameters otherwise. O_{SGL} with an optimal tuning of $\mathcal{F}_*^{(0)} = 10$ reproduces the detection probabilities of the \mathcal{F} -statistic, while O_{SL} and $O_{\text{SGL}}(\mathcal{F}_*^{(0)} = 0)$ have up to 20% lower p_{det} .

For extremely unequal sensitivities, $\sqrt{S^{H2}} = 10\sqrt{S^{H1}}$, as shown in panel (b), the losses of O_{SL} and $O_{\text{SGL}}(\mathcal{F}_*^{(0)} = 0)$ become more pronounced, due to increased false dismissals of 'line-like' signals lowering p_{det} even in the absence of lines. However, $O_{\text{SGL}}(\mathcal{F}_*^{(0)} = 10)$ is *not* affected, because it still lends more weight to the Gaussian-noise hypothesis over the line hypothesis, thus being less likely to confuse signals with lines. This shows that the 'safety'-tuning approach of [1] still works even in this extreme example.

3.2. Lines in the less sensitive detector

For the extreme case of $\sqrt{S^{H2}} = 10\sqrt{S^{H1}}$, lines in the less sensitive detector H2 are already strongly suppressed in the multi-detector \mathcal{F} -statistic, resulting in a population of \mathcal{F} -statistic noise candidates that is quite similar to the case of pure Gaussian noise up to high line SNRs ρ_L .

ROCs for this case, with a line-contamination fraction $f_L^{H2} = 0.1$ and line strength $\rho_L = 6$, are shown in panel (b) of figure 2, compared to the equal-sensitivity case and identical line parameters in panel (a). Whereas the lines in (a) have a strong effect on p_{det} for the various statistics (again similar to the results in [1]), (b) is closer to the Gaussian case (panel (b) of figure 1), with losses in sensitivity for O_{SL} and $O_{\text{SGL}}(\mathcal{F}_*^{(0)} = 0)$, while $O_{\text{SGL}}(\mathcal{F}_*^{(0)} = 10)$ marginally outperforms the \mathcal{F} -statistic.

In figure 3, detection probabilities at fixed $p_{\text{FA}} = 0.001$ are shown for the statistics $2\mathcal{F}$, O_{SL} , $O_{\text{SGL}}(\mathcal{F}_*^{(0)} = 0)$ and $O_{\text{SGL}}(\mathcal{F}_*^{(0)} = 10)$ over a wide range in ρ_S and ρ_L and with a line contamination of $f_L^{H2} = 0.1$.

The results show a very weak dependence on ρ_L . Both the \mathcal{F} -statistic and the line-robust $O_{\text{SGL}}(\mathcal{F}_*^{(0)} = 10)$ perform, over most of the range, as well as in Gaussian noise and for equal sensitivities. The tuned line-robust statistic $O_{\text{SGL}}(\mathcal{F}_*^{(0)} = 10)$ outperforms the \mathcal{F} -statistic only at very high ρ_L .

Meanwhile, O_{SL} and $O_{\text{SGL}}(\mathcal{F}_*^{(0)} = 0)$ show a mostly ρ_L -independent deficiency in detection power, only approaching $p_{\text{det}} = 1$ for extremely high ρ_S of 40 or higher.

3.3. Lines in the more sensitive detector

Next, we consider the case where again $\sqrt{S^{H2}} = 10\sqrt{S^{H1}}$, but now there is a line-contamination fraction in the more sensitive detector of $f_L^{H1} = 0.1$. The ROCs in figure 4 contrast this case (panel b) with the equal-sensitivity case $\sqrt{S^{H2}} = \sqrt{S^{H1}}$ (panel a), both for signals with $\rho_S = 4$ and lines with $\rho_L = 6$. As found before in [1], all variants of the line-robust statistics give large improvements over the \mathcal{F} -statistic in the equal-sensitivity case. However, in panel (b) most of these improvements disappear, though $O_{\text{SGL}}(\mathcal{F}_*^{(0)} = 10)$ is still safe compared to $2\mathcal{F}$ at all p_{FA} .

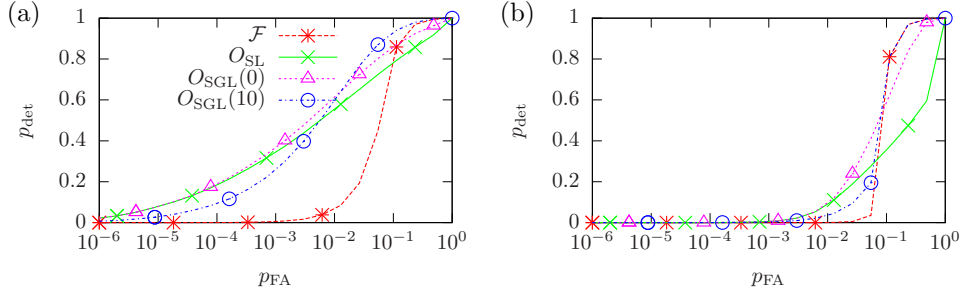


Figure 4. Lines in the more sensitive detector: ROCs for an H1-H2 network, signals with $\rho_S = 4$ and line-contamination fraction $f_L^{H1} = 0.1$, with $\rho_L = 6$. The panels show relative detector sensitivities of (a) $\sqrt{S^{H2}} = \sqrt{S^{H1}}$, (b) $\sqrt{S^{H2}} = 10\sqrt{S^{H1}}$.

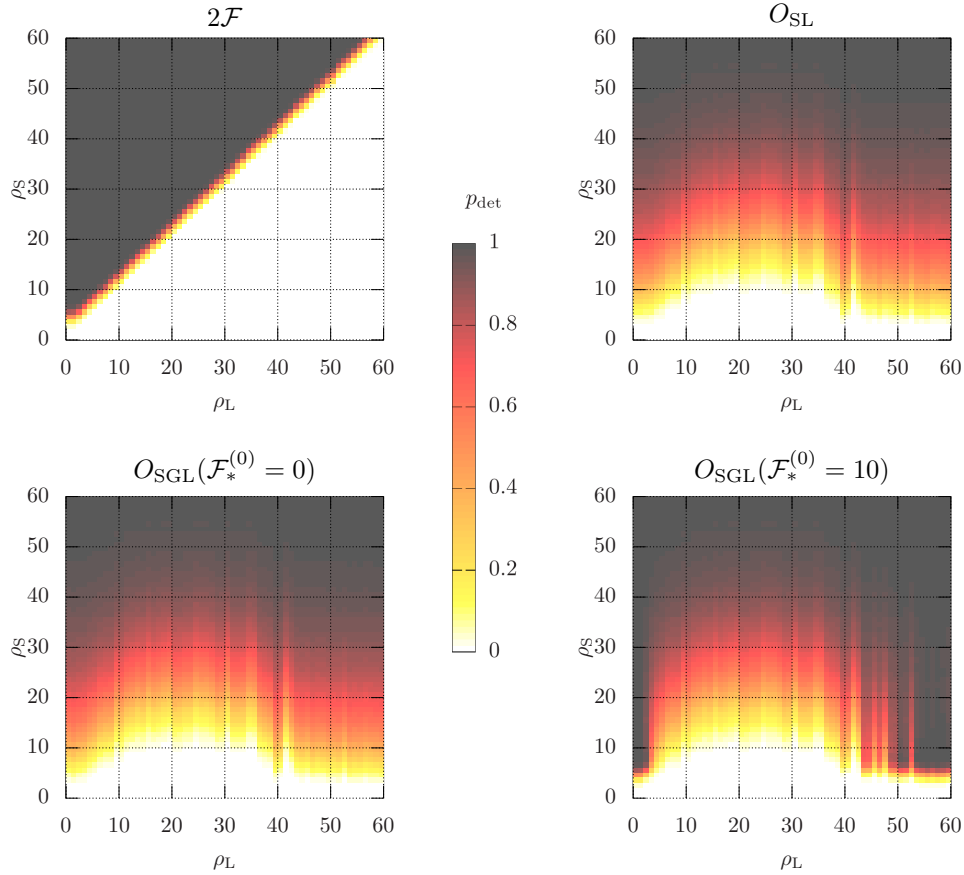


Figure 5. Lines in the more sensitive detector: detection probabilities p_{det} of different statistics, for an H1-H2 network with $\sqrt{S^{H2}} = 10\sqrt{S^{H1}}$, as a function of line SNR ρ_L and signal SNR ρ_S at fixed line contamination $f_L^{H1} = 0.1$ and false-alarm probability $p_{\text{FA}} = 0.001$.

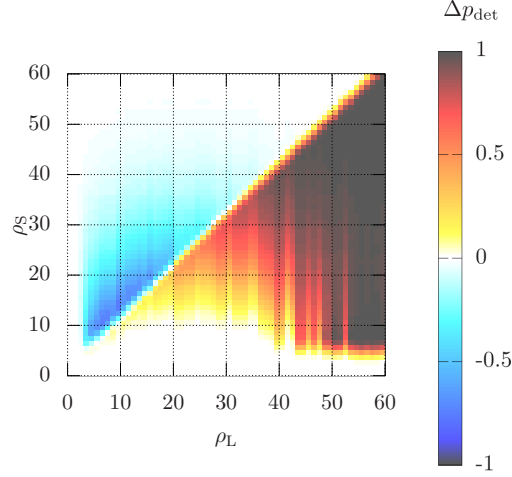


Figure 6. Lines in the more sensitive detector: Detection probability difference $\Delta p_{\text{det}} = p_{\text{det}}(O_{\text{SGL}}) - p_{\text{det}}(2\mathcal{F})$ with $\mathcal{F}_*^{(0)} = 10$, for an H1-H2 network with $\sqrt{S^{\text{H}2}} = 10\sqrt{S^{\text{H}1}}$, as a function of line SNR ρ_L and signal SNR ρ_S , at fixed $f_L^{\text{H}1} = 0.1$ and $p_{\text{FA}} = 0.001$.

A systematic investigation of detection probabilities over a range of ρ_S and ρ_L is shown in figure 5, at fixed $p_{\text{FA}} = 0.001$. This shows that $O_{\text{SGL}}(\mathcal{F}_*^{(0)} = 10)$ performs as well as the \mathcal{F} -statistic at very low ρ_L , where the noise is still almost Gaussian, for all ρ_S . This range also includes the example from figure 4. At very high ρ_L , $O_{\text{SGL}}(\mathcal{F}_*^{(0)} = 10)$ performs much better than \mathcal{F} and almost as well as in the low- ρ_L regime.

In parts of the main region of interest, namely for intermediate to high ρ_L , $O_{\text{SGL}}(\mathcal{F}_*^{(0)} = 10)$ performs worse than the \mathcal{F} -statistic when $\rho_S > \rho_L$. However, this is compensated by regions where $O_{\text{SGL}}(\mathcal{F}_*^{(0)} = 10)$ performs better than $2\mathcal{F}$, namely for $\rho_S < \rho_L$.

A direct comparison of p_{det} between $O_{\text{SGL}}(\mathcal{F}_*^{(0)} = 10)$ and $2\mathcal{F}$ is shown in figure 6. Among the results presented in this section, this plot gives the clearest picture of the potential problem related to the simple line hypothesis introduced in [1]: whereas the line-robust statistics improve over the \mathcal{F} -statistic by suppressing 'signal-like lines', the approach can fail when there are 'line-like signals' in the data because of a much less sensitive detector not picking up the signal.

Typical CW searches with ground-based detectors operate in the regime of low signal SNRs ρ_S , so that the unsafe region for $O_{\text{SGL}}(\mathcal{F}_*^{(0)} = 10)$ is likely of little practical relevance. On the other hand, gains from O_{SGL} in this case are limited to the low- ρ_S and high- ρ_L range, which is more likely to be relevant in real data.

3.4. Sky-location dependence

For differently oriented detectors, their antenna patterns lead to sky-location-dependent sensitivity differences, through the determinant factors D^X (19). However, these differences are quite small, and they partially average out over longer observation times – as visualised in figures A1 and A2. For example, the maximum ratio of antenna-pattern determinants between the H1 and L1 detectors for a 12-hour observation time at any sky location is $D^{L1}/D^{H1} \approx 5.84$. For a 24-hour observation, this decreases to a maximum ratio of $D^{L1}/D^{H1} \approx 2.67$.

In comparing this discrepancy in sensitivities to those considered in the preceding tests, the scale of D^X ratios can be translated to an equivalent scale of square-roots of the noise PSDs. Through the noise-weights of (A.8), D^X is proportional to $(S^X)^{-2}$, so that these maximum ratios would correspond to equivalent square-root-PSD ratios $\sqrt{S^{L1}}/\sqrt{S^{H1}}$ of only about 1.55 and 1.28, respectively.

Hence, we expect only a very small effect on detection probabilities from this most extreme case of different antenna patterns, and even less for other sky locations or for all-sky searches. Synthetic-ROC tests at ‘worst-case’ sky positions have confirmed this, resulting in no significant losses in detection power and no safety concerns for either O_{SGL} or O_{SL} .

4. Sensitivity-weighted detection statistics

In this section, we describe and test an idea for improving the line-robust statistics in the case of detectors with different sensitivities. The idea is to re-weight the contribution of each detector in the denominators of O_{SL} and O_{SGL} with a factor corresponding to its respective sensitivity, including its PSD, the amount of data and sky-location dependence – as seen in (19). By *down-weighting* contributions with higher sensitivity, this should intuitively decrease the chance of considering candidates with unequal \mathcal{F}^X -statistics as lines, thus decreasing the risk of false dismissals. A simple approach for including such a sensitivity weighting consists of changing the amplitude-parameter prior used to derive the likelihood for \mathcal{H}_L (8).

4.1. More on amplitude priors

The derivation of the posterior probability for the signal hypothesis \mathcal{H}_S (5) and \mathcal{H}_L (8) contains an integral for the marginalisation over amplitude parameters \mathcal{A} , namely

$$P(\mathbf{x}|\mathcal{H}_S) = \int P(\mathbf{x}|\mathcal{H}_S, \mathcal{A}) P(\mathcal{A}|\mathcal{H}_S) d\mathcal{A}. \quad (20)$$

As discussed in [15], this integral cannot be solved analytically for general parametrisations of \mathcal{A} and prior distributions $P(\mathcal{A}|\mathcal{H}_S)$. However, as demonstrated in [15, 16], it becomes a simple Gaussian integral for a uniform prior in the four amplitude parameters \mathcal{A}^μ in the ‘JKS factorisation’ (3).

Such a uniform prior would be ‘improper’ (non-normalisable), unless we introduce a cut-off. One possibility is the ‘ \mathcal{F} -statistic prior’ (4) introduced in [16] and adapted in [1], corresponding to a cut-off in a SNR-like quantity $\hat{\rho} \equiv h_0 |\mathcal{M}|^{1/8}$.

However, [15] originally used a different prior distribution, placing a fixed cut-off $h_{\text{max}} \in (0, \infty)$ on the signal-strength parameter h_0 :

$$P(\{\mathcal{A}^\mu\}|\mathcal{H}_{\mathcal{S}\mathcal{M}}) = \begin{cases} C & \text{for } h_0(\mathcal{A}) < h_{\max}, \\ 0 & \text{otherwise.} \end{cases} \quad (21)$$

Here, we use $\mathcal{H}_{\mathcal{S}\mathcal{M}}$ as a shorthand for this signal hypothesis with modified amplitude prior.

This variant was discarded in [16] due to poor performance of the resulting detection statistic on medium-duration ‘transient CW’ signals. However, for standard CW signals, the effect of such a prior has not been explicitly analysed yet, especially not in the context of comparing several detectors for robustness against line artefacts.

4.2. Sensitivity weighting for signals in pure Gaussian noise?

Before considering lines, it clarifies matters to first investigate the effect of these prior choices in the simpler case of CW signals in pure Gaussian noise. The difference between the two prior choices is that (4) results in the signal-hypothesis posterior (5)

$$P(\mathcal{H}_S|\mathbf{x}) = o_{\text{SG}} c_*^{-1} P(\mathcal{H}_G|\mathbf{x}) e^{\mathcal{F}(\mathbf{x})} \quad (22)$$

and in signal-to-Gaussian-noise odds (12) of $O_{\text{SG}}(\mathbf{x}) \propto e^{\mathcal{F}(\mathbf{x})}$, while (21) leads to a signal-hypothesis posterior

$$P(\mathcal{H}_{\mathcal{S}\mathcal{M}}|\mathbf{x}) = o_{\mathcal{S}\mathcal{M}\text{G}} \frac{70}{h_{\max}^4} P(\mathcal{H}_G|\mathbf{x}) |\mathcal{M}|^{-1/2} e^{\mathcal{F}(\mathbf{x})} \quad (23)$$

and odds of

$$O_{\mathcal{S}\mathcal{M}\text{G}}(\mathbf{x}) \equiv \frac{P(\mathcal{H}_{\mathcal{S}\mathcal{M}}|\mathbf{x})}{P(\mathcal{H}_G|\mathbf{x})} \propto |\mathcal{M}|^{-1/2} e^{\mathcal{F}(\mathbf{x})}. \quad (24)$$

As discussed before, the antenna-pattern determinant $|\mathcal{M}|$ is a measure of the overall sensitivity of a network of detectors. We therefore refer, in the following, to any statistic derived from the prior (21), so that it has an explicit factor of $|\mathcal{M}|$ in the odds, as a *sensitivity-weighted statistic*.

Inserting the explicit expression from (18) yields

$$O_{\mathcal{S}\mathcal{M}\text{G}}(\mathbf{x}) \propto e^{\mathcal{F}(\mathbf{x})} \mathcal{S}^2 T_{\text{data}}^{-2} D^{-1}, \quad (25)$$

demonstrating that any candidate coming from a particularly good set of data (low \mathcal{S} , large T_{data}), or from a point on the sky where the detector is most sensitive over the observation time (large D), is actually *down-weighted*. Thus, intuitively this statistic should be worse than the pure \mathcal{F} -statistic, and hence we will not use $\mathcal{H}_{\mathcal{S}\mathcal{M}}$ instead of \mathcal{H}_S .

4.3. Sensitivity-weighted line-veto statistic

On the other hand, the effect of down-weighting outliers from more sensitive data could be useful in the case of line-vetoing. Consider again two detectors, one much more sensitive than the other (e.g., having lower S^X), and a signal that is strong enough to produce an elevated \mathcal{F}^X -statistic in the better detector, but not strong enough to be seen in the other one. This signal is likely to trigger the simple line hypothesis \mathcal{H}_L from [1], as the signature is similar to that of a line in one of two equally sensitive detectors.

When we introduce sensitivity weighting in a modified line hypothesis, an outlier in the more sensitive detector will be considered less likely to come from a line. Such a reduction of false positives for the line hypothesis should then lead to less false dismissals of signals by the signal-versus-line odds.

Hence, we define a sensitivity-weighted single-detector line hypothesis $\mathcal{H}_{\text{LM}}^X$ that uses the single-detector version of the prior from (21):

$$P(\{\mathcal{A}^{X\mu}\}|\mathcal{H}_{\text{LM}}^X) = \begin{cases} C & \text{for } h_0(\mathcal{A}^X) < h_{\text{max}}^X, \\ 0 & \text{otherwise.} \end{cases} \quad (26)$$

The line hypothesis \mathcal{H}_{LM} for a non-coincident line in any detector is constructed as in equation (19) of [1]. *Sensitivity-weighted line-veto odds* are then given by the unweighted signal hypothesis \mathcal{H}_S and the weighted \mathcal{H}_{LM} :

$$O_{\text{SLM}}(\mathbf{x}) \equiv \frac{P(\mathcal{H}_S|\mathbf{x})}{P(\mathcal{H}_{\text{LM}}|\mathbf{x})} = o_{\text{SLM}} \frac{\hat{\rho}_{\text{max}}^{-4} e^{\mathcal{F}(\mathbf{x})}}{\left\langle (h_{\text{max}}^X)^{-4} r^X |\mathcal{M}^X|^{-1/2} e^{\mathcal{F}^X(x^X)} \right\rangle_X}, \quad (27)$$

where r^X are the line-prior weights defined in (10).

This expression contains various prior-cut-off parameters: $\hat{\rho}_{\text{max}}$ from \mathcal{H}_S and a set of $\{h_{\text{max}}^X\}$ from $\mathcal{H}_{\text{LM}}^X$. In [1], $\hat{\rho}_{\text{maxS}} = \hat{\rho}_{\text{maxL}} = \hat{\rho}_{\text{maxL}}^X$ was assumed for all X , so that any such parameters cancelled out. Here, we first assume $h_{\text{max}}^X = h_{\text{max}}$, again for all X , justified by the general absence of detailed physical knowledge about different line-strength populations in different detectors. This reduces the effect of the cut-offs to a common pre-factor to the odds:

$$O_{\text{SLM}}(\mathbf{x}) = o_{\text{SLM}} \left(\frac{h_{\text{max}}}{\hat{\rho}_{\text{max}}} \right)^4 \frac{e^{\mathcal{F}(\mathbf{x})}}{\left\langle r^X |\mathcal{M}^X|^{-1/2} e^{\mathcal{F}^X(x^X)} \right\rangle_X}. \quad (28)$$

As the only requirement for these cut-offs is that they should be large enough for the marginalisation integral to become Gaussian, we can choose to keep only one of them as a free parameter and to fix the ratio between them. For convenience of notation, we define

$$\mathcal{D} \equiv \left(\frac{\hat{\rho}_{\text{max}}}{h_{\text{max}}} \right)^8 = \text{const.} \quad (29)$$

Pulling \mathcal{D} into the denominator and defining a per-detector relative *sensitivity-weighting factor*

$$q^X \equiv \sqrt{\frac{\mathcal{D}}{|\mathcal{M}^X|}}, \quad (30)$$

the weighted line-veto statistic (27) becomes

$$O_{\text{SLM}}(\mathbf{x}) = o_{\text{SLM}} \frac{e^{\mathcal{F}(\mathbf{x})}}{\left\langle r^X q^X e^{\mathcal{F}^X(x^X)} \right\rangle_X}. \quad (31)$$

4.4. Sensitivity-weighted line-robust statistic

Furthermore, we construct an extended noise hypothesis, in analogy to equation (32) of [1], but this time using the modified line-amplitude prior from (26):

$$\mathcal{H}_{\text{GLM}} : (\mathcal{H}_G \text{ or } \mathcal{H}_{\text{LM}}). \quad (32)$$

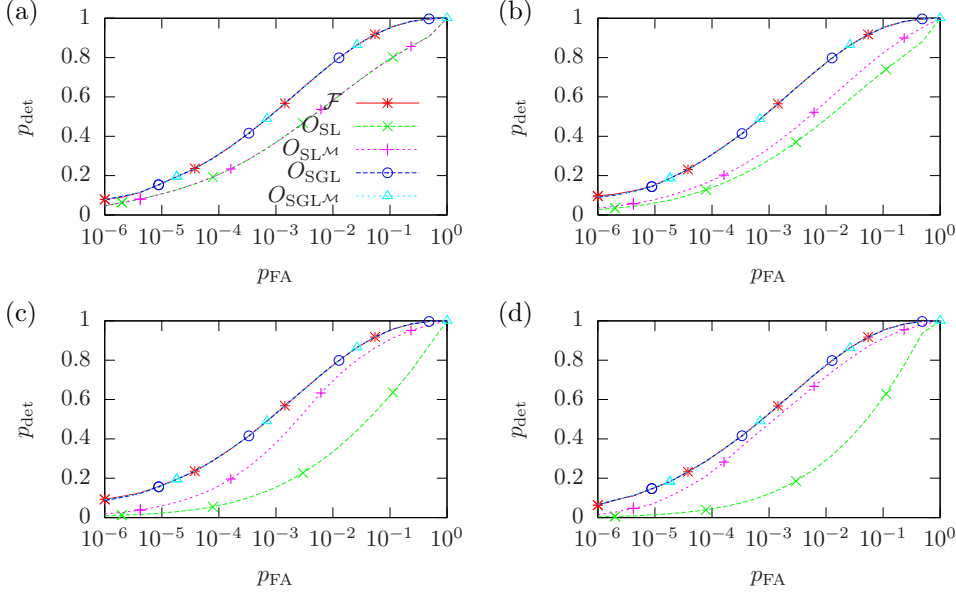


Figure 7. ROCs for signals with $\rho_S = 4$ in pure Gaussian noise. The panels show relative detector sensitivities of (a) $\sqrt{S^{H2}} = \sqrt{S^{H1}}$, (b) $\sqrt{S^{H2}} = 2\sqrt{S^{H1}}$, (c) $\sqrt{S^{H2}} = 5\sqrt{S^{H1}}$, (d) $\sqrt{S^{H2}} = 10\sqrt{S^{H1}}$. O_{SGL} and O_{SGL^M} both use $\mathcal{F}_*^{(0)} = 10$.

This gives the *sensitivity-weighted line-robust odds* as an analogue to O_{SGL} of (14):

$$O_{SGL^M}(\mathbf{x}) \equiv \frac{P(\mathcal{H}_S|\mathbf{x})}{P(\mathcal{H}_{GL^M}|\mathbf{x})} = o_{SGL^M} \frac{e^{\mathcal{F}(\mathbf{x})}}{(1 - p_L) e^{\mathcal{F}_*^{(0)}} + p_L \langle r^X q^X e^{\mathcal{F}^X(x^X)} \rangle_X}. \quad (33)$$

Here, the transition-scale parameter $\mathcal{F}_*^{(0)}$ is unchanged from its definition in (16), as only the per-detector terms are modified.

Comparing the relative scale between the constant term and the per-detector terms, a change in sensitivity-weighting factors q^X would only be compensated by a logarithmic change in $\mathcal{F}_*^{(0)}$. If we further choose the free parameter \mathcal{D} as similar to typical $|\mathcal{M}^X|$ values, all denominator terms in (33) become similar in scale to those in (14). In principle, \mathcal{D} should be a constant over the whole parameter space, but as the sky-dependent variations in D^X , and thus $|\mathcal{M}^X|$, are rather small, we choose a particularly simple prescription:

$$\mathcal{D}(\alpha, \delta) \equiv \langle |\mathcal{M}^X(\alpha, \delta)| \rangle_X = \mathcal{S}^{-4} \langle (T_{\text{data}}^X)^4 (D^X(\alpha, \delta))^2 \rangle_X. \quad (34)$$

With this convention, an empirical tuning of $\mathcal{F}_*^{(0)}$, as described in section VI.B of [1], can be expected to yield similar values as for the unweighted O_{SGL} . Numerical tests indeed show only small changes in the optimal $\mathcal{F}_*^{(0)}$ over typical ranges in false-alarm probabilities.

4.5. Synthetic tests of the sensitivity-weighted statistics

In this section, we present results from synthetic-draw comparisons of the sensitivity-weighted detection statistics $O_{\text{SL}\mathcal{M}}$ and $O_{\text{SGL}\mathcal{M}}$ against their unweighted counterparts O_{SL} and O_{SGL} , covering a similar range of noise populations as in section 3.

4.5.1. Gaussian noise

To determine the effect of sensitivity-weighting on the detection performance of the line-robust statistics, we first revisit the same case as covered in figure 1, but including additional sensitivity ratios. For a colocated network of H1 and H2, signals with $\rho_{\text{S}} = 4$ and pure Gaussian noise, the corresponding set of ROCs is shown in figure 7.

Panel (a) of figure 7 shows the case of equal sensitivity, where $O_{\text{SL}\mathcal{M}}$ and $O_{\text{SGL}\mathcal{M}}(\mathcal{F}_*^{(0)} = 10)$ perform exactly as their unweighted counterparts. This is expected from the analytical expressions in (31) and (33), as in this case $q^X = 1$ and so the statistics revert back to the unweighted forms, (13) and (14).

For increasing ratios of $\sqrt{S^{\text{H2}}}/\sqrt{S^{\text{H1}}} \in \{2, 5, 10\}$ (panels (b)–(d) of figure 7), there is still no difference between O_{SGL} and $O_{\text{SGL}\mathcal{M}}$ with both at $\mathcal{F}_*^{(0)} = 10$. However, p_{det} for the unweighted O_{SL} decreases, while $O_{\text{SL}\mathcal{M}}$ actually improves and approaches the performance of $2\mathcal{F}$ and $O_{\text{SGL}}(\mathcal{F}_*^{(0)} = 10)$. ROCs for intermediate values of $\mathcal{F}_*^{(0)}$ would fall between the curves for O_{SL} (which corresponds to $\mathcal{F}_*^{(0)} \rightarrow -\infty$) and $\mathcal{F}_*^{(0)} = 10$.

4.5.2. Lines in the less sensitive detector

The case of an H1-H2 network with $\sqrt{S^{\text{H2}}} = 10\sqrt{S^{\text{H1}}}$ and a line contamination of $f_{\text{L}}^{\text{H2}} = 0.1$ in the weaker detector was considered before in section 3.2 for the unweighted statistics, and the results were similar to pure Gaussian noise: significant losses in p_{det} for O_{SL} and O_{SGL} for low $\mathcal{F}_*^{(0)}$, while $O_{\text{SGL}}(\mathcal{F}_*^{(0)} = 10)$ in this case is still completely safe when compared to the \mathcal{F} -statistic.

To illustrate the effect of sensitivity weighting for this noise population, figure 8 shows differences of p_{det} between weighted and unweighted statistics over the same range in ρ_{S} and ρ_{L} as in figure 3. Similarly to the Gaussian-noise ROCs in figure 7, $O_{\text{SL}\mathcal{M}}$ and $O_{\text{SGL}\mathcal{M}}(\mathcal{F}_*^{(0)} = 0)$ can regain 20-30% of p_{det} in comparison to their unweighted counterparts, whereas for high $\mathcal{F}_*^{(0)}$ such as 10 the changes are negligible.

4.5.3. Lines in the more sensitive detector

On the other hand, as we have already seen in figure 4, the detection problem is more difficult in general if there are lines present in the more sensitive detector. These can be very hard to distinguish from CW signals with only the information in $\{\mathcal{F}, \mathcal{F}^X\}$.

For the same parameters as in figure 5, i.e. an H1-H2 network with $\sqrt{S^{\text{H2}}} = 10\sqrt{S^{\text{H1}}}$ and a line contamination of $f_{\text{L}}^{\text{H1}} = 0.1$, changes in p_{det} due to sensitivity-weighting are shown in figure 9. In these noise populations, the improvements of the sensitivity-weighted counterparts to O_{SL} and O_{SGL} with low $\mathcal{F}_*^{(0)}$ are more modest than in the previous cases, with p_{det} improving only in the low- and high- ρ_{L} regions, and not in the most problematic range in-between. Sensitivity weighting again brings no improvement for an optimally-tuned $O_{\text{SGL}}(\mathcal{F}_*^{(0)} = 10)$.

4.5.4. Sky-location dependence

We have also compared synthetic ROCs for the weighted and unweighted statistics

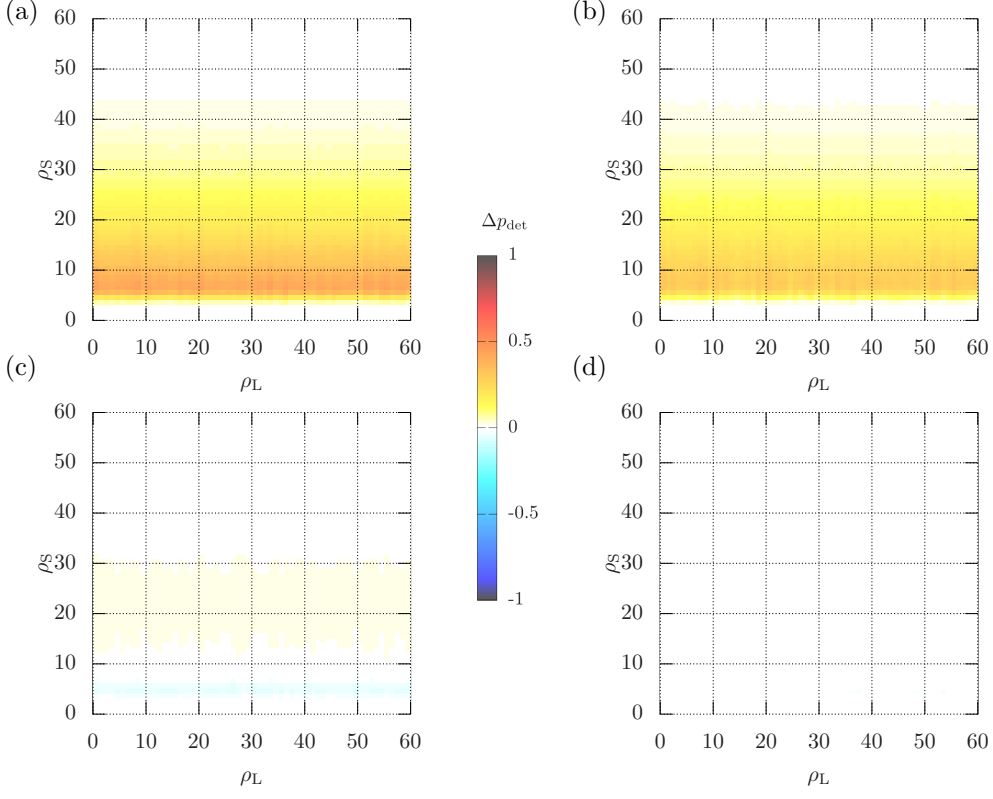


Figure 8. Lines in the less sensitive detector: Detection-probability differences between weighted and unweighted statistics, for an H1-H2 network with $\sqrt{S^{\text{H2}}} = 10\sqrt{S^{\text{H1}}}$, as a function of line SNR ρ_L and signal SNR ρ_S , at fixed $f_L^{\text{H2}} = 0.1$ and $p_{\text{FA}} = 0.001$.

- (a): $p_{\text{det}}(O_{\text{SL}\mathcal{M}}) - p_{\text{det}}(O_{\text{SL}})$, (b): $p_{\text{det}}(O_{\text{SGL}\mathcal{M}}) - p_{\text{det}}(O_{\text{SGL}})$ at $\mathcal{F}_*^{(0)} = 0$,
 (c): $p_{\text{det}}(O_{\text{SGL}\mathcal{M}}) - p_{\text{det}}(O_{\text{SGL}})$ at $\mathcal{F}_*^{(0)} = 4$, (d): $p_{\text{det}}(O_{\text{SGL}\mathcal{M}}) - p_{\text{det}}(O_{\text{SGL}})$ at $\mathcal{F}_*^{(0)} = 10$.

for a non-colocated network of H1 and L1 at the ‘worst-case’ different-sensitivity sky locations discussed in section 3.4.

For $T_{\text{obs}} = 12$ h, the differences are already negligible in pure Gaussian noise and small, at most a few percent, in the presence of lines in either detector. All differences are completely negligible for $T_{\text{obs}} = 24$ h.

5. Conclusions

The synthetic tests presented in this paper lead to the following main conclusions about the safety of line-robust statistics for unequally sensitive detectors, and about the simple sensitivity-weighting attempt to improving it:

- (i) The sky-location-dependent differences in detector sensitivities, due to different antenna patterns, are generally too small to lead to any noticeable effects. Even for a search over a short observation time of 12 h and directed at a location with extreme differences in antenna patterns, the effect on detection probabilities is

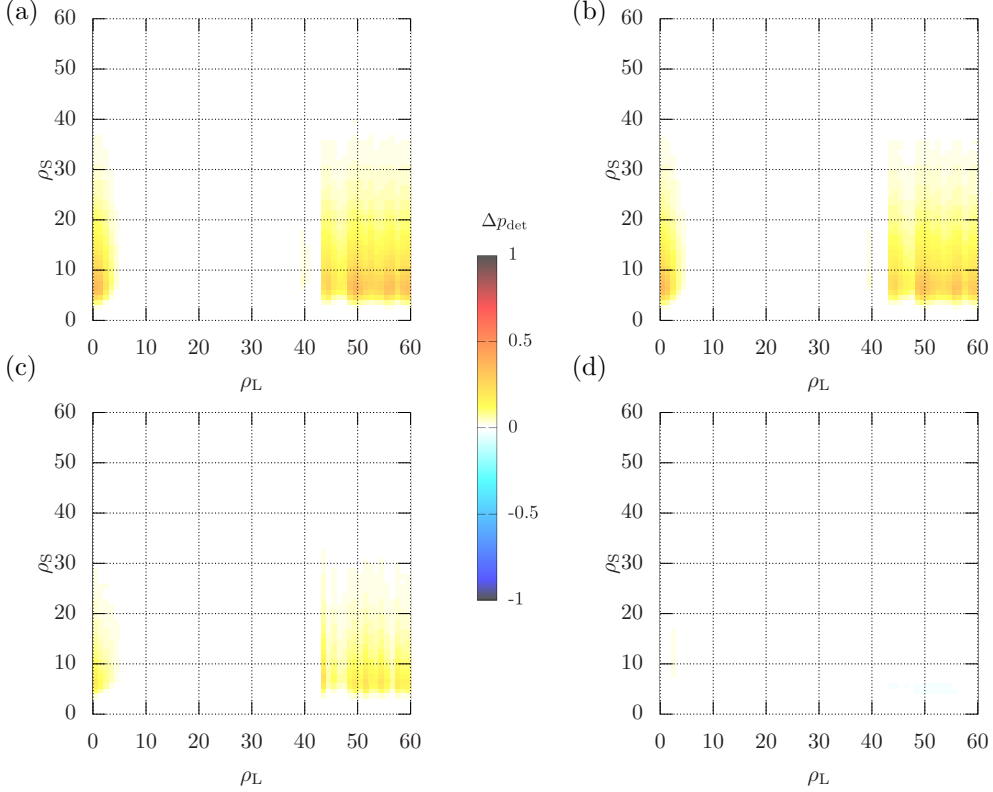


Figure 9. Lines in the more sensitive detector: Detection probability differences between weighted and unweighted statistics, for an H1-H2 network with $\sqrt{S^{\text{H}2}} = 10\sqrt{S^{\text{H}1}}$, as a function of line SNR ρ_L and signal SNR ρ_S , at fixed $f_L^{\text{H}1} = 0.1$ and $p_{\text{FA}} = 0.001$.

- (a): $p_{\text{det}}(O_{\text{SL}\mathcal{M}}) - p_{\text{det}}(O_{\text{SL}})$, (b): $p_{\text{det}}(O_{\text{SGL}\mathcal{M}}) - p_{\text{det}}(O_{\text{SGL}})$ at $\mathcal{F}_*^{(0)} = 0$,
(c): $p_{\text{det}}(O_{\text{SGL}\mathcal{M}}) - p_{\text{det}}(O_{\text{SGL}})$ at $\mathcal{F}_*^{(0)} = 4$, (d): $p_{\text{det}}(O_{\text{SGL}\mathcal{M}}) - p_{\text{det}}(O_{\text{SGL}})$ at $\mathcal{F}_*^{(0)} = 10$.

small. Hence, the line-robust detection statistics from [1] can be considered as just as safe for directed searches as for the all-sky searches tested before, provided the detectors have similar noise PSDs and amounts of data.

- (ii) To notice any effects due to unequal sensitivities, these must be quite pronounced, for example a ratio in $\sqrt{S^X}$ of well over 2, which is larger than typical values encountered for the LIGO H1-L1 network.
- (iii) Even for very unequal sensitivities (for example a factor 10 in $\sqrt{S^X}$), the line-robust statistic O_{SGL} of (14) with an $\mathcal{F}_*^{(0)}$ -tuning as described in section VI.B of [1] is still *safe* in Gaussian noise – in the sense of not being worse than the \mathcal{F} -statistic – and improves over \mathcal{F} in the presence of strong lines in a less sensitive detector only.
- (iv) The line-veto statistic O_{SL} of (13), as well as O_{SGL} with lower values of $\mathcal{F}_*^{(0)}$, are *not safe* in these cases. Here, sensitivity-weighting can recover some losses. However, there would normally be no reason to use these statistics in place of the tuned O_{SGL} , for which sensitivity-weighting makes no significant difference in

any of the cases considered here.

- (v) For very unequal sensitivities, lines in the most sensitive detector lead to partial losses and partial gains of the tuned O_{SGL} compared to the \mathcal{F} -statistic. The cases where O_{SGL} is unsafe (at high signal SNRs) are arguably of less practical relevance than those where it still yields an improvement (for weaker signals and very strong lines). Again, sensitivity-weighting makes no difference to the performance of the tuned O_{SGL} .

Thus, we find that the sensitivity-weighting approach through the use of a modified amplitude prior, as described in section 4, does not seem a promising direction in practice. The “unweighted” but tuned line-robust statistic, as described in [1], is generally found to be safe even for detectors with highly unequal sensitivities. The remaining weakness for particularly “line-like signals” might be a subject for further work, although the quantitative limits demonstrated here make this seem less urgent for practical applications.

Acknowledgements

We thank the following colleagues for insightful discussions and comments: Bruce Allen, Berit Behnke, Heinz-Bernd Eggenstein, Maria Alessandra Papa, Keith Riles, Karl Wette, John T. Whelan and Graham Woan. DK was supported by the IMPRS on Gravitational Wave Astronomy. This paper has been assigned LIGO document number LIGO-P1400161 and AEI-preprint number AEI-2014-039.

Appendix A. Details on antenna patterns

For reference, here we give the full expressions for the antenna-pattern matrix and functions, following the notation of [26].

Consider a GW propagating in the direction of the normal vector $-\hat{n}$ in a reference frame fixed in the solar system barycentre (SSB), with an axis \hat{z} orthogonal to the equatorial plane. Then, the propagating wave frame is given by unit vectors

$$-\hat{n}, \quad \hat{\xi} = \hat{n} \times \hat{z} / |\hat{n} \times \hat{z}| \quad \text{and} \quad \hat{\eta} = \hat{\xi} \times \hat{n} \quad (\text{A.1})$$

and polarisation tensors

$$\epsilon_+ = \hat{\xi} \otimes \hat{\xi} - \hat{\eta} \otimes \hat{\eta} \quad (\text{A.2})$$

$$\epsilon_\times = \hat{\xi} \otimes \hat{\eta} + \hat{\eta} \otimes \hat{\xi}. \quad (\text{A.3})$$

For a detector X whose position on the earth’s surface is given, again in SSB coordinates, by the tensor d^X , the two antenna pattern functions corresponding to the two polarisation components are then given, in the long-wavelength limit, by

$$a^X(t, \hat{n}) \equiv d_{ij}^X(t) \epsilon_+^{ij}(\hat{n}), \quad (\text{A.4})$$

$$b^X(t, \hat{n}) \equiv d_{ij}^X(t) \epsilon_\times^{ij}(\hat{n}). \quad (\text{A.5})$$

The antenna-pattern matrix components A , B , C of (17) are defined as *noise-weighted* averages over *Short Fourier Transforms* (SFTs):

$$\begin{aligned} A &= \langle a^2(t) \rangle_{\text{SFTs}}, \\ B &= \langle b^2(t) \rangle_{\text{SFTs}}, \\ C &= \langle a(t) b(t) \rangle_{\text{SFTs}}. \end{aligned} \quad (\text{A.6})$$

The averages are performed according to

$$\langle Q \rangle_{\text{SFTs}} = \frac{1}{N_{\text{SFT}}} \sum_{X=1}^{N_{\text{det}}} \sum_{\alpha=1}^{N_{\text{SFT}}} w_{X\alpha} Q_{X\alpha}, \quad (\text{A.7})$$

with per-SFT and per-detector *noise-weights* factors

$$w_{X\alpha} = \frac{\mathcal{S}}{S_{\alpha}^X} \quad (\text{A.8})$$

which fulfil the normalisation constraint

$$\sum_{X\alpha} w_{X\alpha} = \sum_X N_{\text{SFT}}^X = N_{\text{SFT}}. \quad (\text{A.9})$$

Notably, for single-detector quantities Q^X , we could use noise-weights normalised by S^X instead of \mathcal{S} ; however, the convention of [26] and current LALSuite implementations [‡] is to use the same averaging as for multi-detector quantities:

$$\langle Q^X \rangle_{\text{SFTs}} = \frac{1}{N_{\text{SFT}}^X} \sum_{\alpha=1}^{N_{\text{SFT}}^X} w_{X\alpha} Q_{\alpha}^X, \quad (\text{A.10})$$

so that

$$\begin{aligned} A^X &= \frac{1}{N_{\text{SFT}}^X} \sum_{\alpha=1}^{N_{\text{SFT}}^X} w_{X\alpha} a^{X2}(t) \\ B^X &= \frac{1}{N_{\text{SFT}}^X} \sum_{\alpha=1}^{N_{\text{SFT}}^X} w_{X\alpha} b^{X2}(t) \\ C^X &= \frac{1}{N_{\text{SFT}}^X} \sum_{\alpha=1}^{N_{\text{SFT}}^X} w_{X\alpha} a^X(t) b^X(t). \end{aligned} \quad (\text{A.11})$$

This normalisation means that the per-detector antenna-pattern matrix determinants are again given by multiplying with the *multi*-detector sensitivity and data volume:

$$|\mathcal{M}^X| = (\mathcal{S}^{-1} T_{\text{data}})^4 D^{X2}. \quad (\text{A.12})$$

Although this quantity is invariant under a normalisation change like, for example,

$$w_{X\alpha} \rightarrow w'_{X\alpha} = \frac{S^X}{S_{\alpha}^X}, \quad (\text{A.13})$$

the A^X , B^X , C^X and D^X are not, and the determinant transforms as

$$|\mathcal{M}^X| = (\mathcal{S}^{-1} T_{\text{data}})^4 D^{X2} = \left(\frac{T_{\text{data}}^X}{S^X} \right)^4 D'^{X2}. \quad (\text{A.14})$$

In figure A1, we see a sky-map of D for four different detectors (LIGO H1 in Hanford, Washington, USA; LIGO L1 in Livingston, Louisiana, USA; GEO600 near Hannover, Germany and Virgo in Cascina, Italy) averaged over 12 hours.

In contrast, figure A2 adds another 12 hours. We see that for a whole day of observation (or integer multiples thereof), most of the variation in right ascension α is averaged away.

[‡] <https://www.lsc-group.phys.uwm.edu/daswg/projects/lalsuite.html>

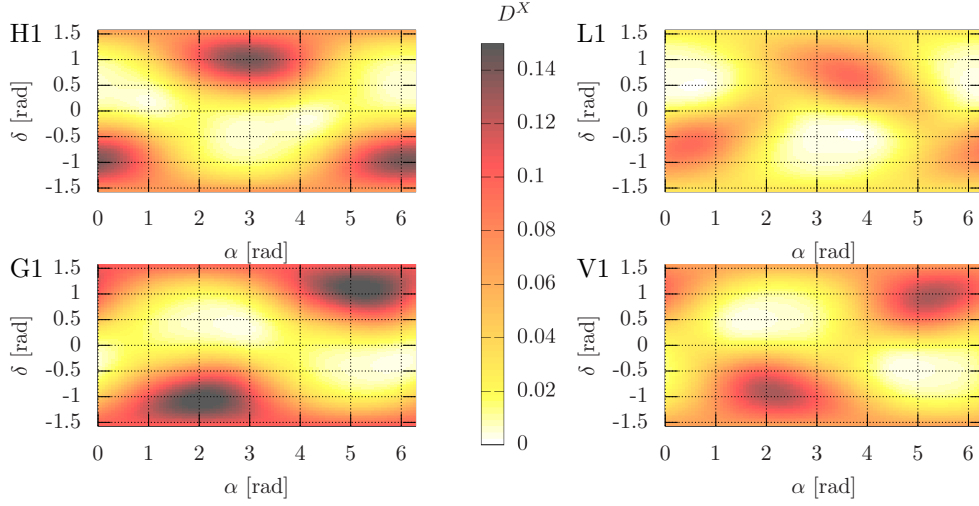


Figure A1. Per-detector antenna pattern matrix determinant D^X (colour scale) over the sky (α, δ in rectangular projection) averaged over 12 hours (24 SFTs) starting from GPS time 852443819 (Jan 10, 2007, 05:56:45 UTC; during the LIGO S5 run) for LIGO Hanford (H1), LIGO Livingston (L1), GEO600 (Hannover, G1), Virgo (Cascina, V1).

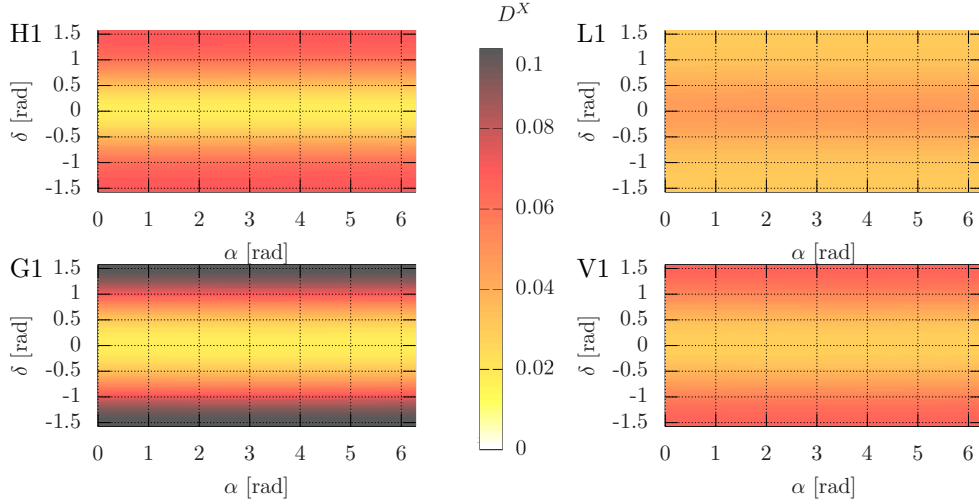


Figure A2. Per-detector antenna pattern matrix determinant D^X (colour scale) over the sky (α, δ in rectangular projection) averaged over 24 hours (48 SFTs) starting from GPS time 852443819 (Jan 10, 2007, 05:56:45 UTC; during the LIGO S5 run) for LIGO Hanford (H1), LIGO Livingston (L1), GEO600 (Hannover, G1), Virgo (Cascina, V1). Note that the small remaining α -dependence would only average out over a *sidereal* day (≈ 23.9344 hours) and using finer time resolution.

References

- [1] Keitel D, Prix R, Papa M A, Leaci P and Siddiqi M 2014 *Phys. Rev. D* **89** 064023 [arXiv:1311.5738]
- [2] Prix R (for the LSC) 2009 Gravitational waves from spinning neutron stars *Neutron Stars and Pulsars (Astrophysics and Space Science Library* vol 357) ed Becker W (Springer Berlin Heidelberg) p 651 ISBN 978-3-540-76964-4 (LIGO-P060039-v3) URL <https://dcc.ligo.org/LIGO-P060039/public>
- [3] Owen B J, Reitze D H and Whitcomb S E 2009 Probing neutron stars with gravitational waves *astro2010: The Astronomy and Astrophysics Decadal Survey* p 229 [arXiv:0903.2603]
- [4] Abbott B P *et al.* (LIGO Scientific Collaboration) 2009 *Rep. Prog. Phys.* **72** 076901 [arXiv:0711.3041]
- [5] Accadia T *et al.* 2011 *Class. Quant. Grav.* **28** 114002
- [6] Grote H (for the LIGO Scientific Collaboration) 2010 *Class. Quant. Grav.* **27** 084003
- [7] Bildsten L 1998 *Astrophys. J. Lett.* **501** L89 [arXiv:astro-ph/9804325]
- [8] Ushomirsky G, Cutler C and Bildsten L 2000 *Mon. Not. R. Astron. Soc.* **319** 902–932 [arXiv:astro-ph/0001136]
- [9] Johnson-McDaniel N K and Owen B J 2013 *Phys. Rev. D* **88** 044004 [arXiv:1208.5227]
- [10] Abbott B *et al.* (LIGO Scientific Collaboration) 2004 *Phys. Rev. D* **69** 082004 [arXiv:gr-qc/0308050]
- [11] Aasi J *et al.* (LIGO Scientific Collaboration and Virgo Collaboration) 2013 *Phys. Rev. D* **87** 042001 [arXiv:1207.7176]
- [12] Behnke B 2013 *A Directed Search for Continuous Gravitational Waves from Unknown Isolated Neutron Stars at the Galactic Center* Ph.D. thesis Hannover University URL <http://opac.tib.uni-hannover.de/DB=1/XMLPRS=N/PPN?PPN=752172840>
- [13] Jaranowski P, Królak A and Schutz B F 1998 *Phys. Rev. D* **58** 063001 [arXiv:gr-qc/9804014]
- [14] Cutler C and Schutz B F 2005 *Phys. Rev. D* **72** 063006 [arXiv:gr-qc/0504011]
- [15] Prix R and Krishnan B 2009 *Class. Quant. Grav.* **26** 204013 [arXiv:0907.2569]
- [16] Prix R, Giampanis S and Messenger C 2011 *Phys. Rev. D* **84** 023007 [arXiv:1104.1704]
- [17] Whelan J T, Prix R, Cutler C J and Willis J L 2014 *Class. Quant. Grav.* **31** 065002 [arXiv:1311.0065]
- [18] Christensen N (for the LVC) 2010 *Class. Quant. Grav.* **27** 194010
- [19] Coughlin M (for the LVC) 2010 *J. Phys. Conf. Ser.* **243** 012010 [arXiv:1109.0330]
- [20] Aasi J *et al.* (LIGO Scientific Collaboration and Virgo Collaboration) 2012 *Class. Quant. Grav.* **29** 155002 [arXiv:1203.5613]
- [21] Accadia T *et al.* 2012 *J. Phys. Conf. Ser.* **363** 012037
- [22] Aasi J *et al.* (LIGO Scientific Collaboration and Virgo Collaboration) 2014 [arXiv:1410.7764]
- [23] Aasi J *et al.* (LIGO Scientific Collaboration and Virgo Collaboration) 2013 *Phys. Rev. D* **88** 102002 [arXiv:1309.6221]
- [24] Behnke B, Papa M A and Prix R 2014 [arXiv:1410.5997]
- [25] Prix R 2007 *Phys. Rev. D* **75** 023004 [arXiv:gr-qc/0606088]
- [26] Prix R 2010 *The F-statistic and its implementation in ComputeFStatistic_v2* Tech. rep. LIGO Scientific Collaboration (LIGO-T0900149-v3) URL <https://dcc.ligo.org/LIGO-T0900149-v3/public>